Vacancy-hydrogen defects in silicon studied by Raman spectroscopy

E. V. Lavrov* and J. Weber
Institute for Low Temperature Physics, TU Dresden, 01062 Dresden, Germany

L. Huang
Department of MEMS, Duke University, Durham, North Carolina 27708

B. Bech Nielsen
Institute of Physics and Astronomy, Universtity of Århus, DK-8000, Århus, Denmark
(Received 19 March 2001; published 21 June 2001)

A Raman study of hydrogen stretching modes in vacancy-hydrogen defects (VH_n, $n=1,2,3,4$) is presented. The positions of the vibrational modes are compared to recent IR absorption results. The Raman lines exhibit pronounced polarization due to the $\langle 111\rangle$ orientation of the silicon-hydrogen bond. Based on the defect symmetry derived from the polarization-dependent Raman signals and the Raman intensities we assign the Raman lines to the defects VH_4: 2234 cm^{-1}(A_1 mode), 2205 cm^{-1} (T_2 mode); V_2H_6: 2180 cm^{-1} (A_{1g} mode), 2155 cm^{-1} (E_g mode). We tentatively attribute the 2120- and 2099-cm^{-1} lines to VH_2 and the 2022-cm^{-1} line to VH.

DOI: 10.1103/PhysRevB.64.035204 PACS number(s): 61.72.Ji, 63.20.Pw, 78.30.Am

I. INTRODUCTION

Hydrogen-related defects in silicon have been investigated extensively for the last two decades.[1,2] From theoretical and experimental studies a model for the vacancy-hydrogen defects, with a single vacancy and up to four hydrogen atoms (VH_n with $n=1,2,3,4$) was developed.[3–14] In these defects the Si–H bonds point almost along the $\langle 111\rangle$ directions towards the center of the vacancy. The Si–H bonds become shorter with increasing hydrogen numbers due to the mutual repulsion between the hydrogen atoms, which leads to an increase in the frequencies of the Si–H local vibrational modes (LVM's) going from VH to VH_4. The properties of individual VH_n can be summarized as follows.

VH: The defect is paramagnetic in the neutral charge state, has C_{3v} (trigonal) symmetry, and is stable up to 200 °C in proton implanted material.[13,14] Based on the correlation of the annealing curves of the electron paramagnetic resonance (EPR) signal with that of the infrared absorption line at 2038.5 cm^{-1} measured at 10 K, the latter has been tentatively assigned to a stretch LVM of VH^0.[15]

VH_2: Fourier transform infrared (FTIR) absorption measurements have shown that VH_2 has C_{2v} (orthorhombic I) symmetry and possesses two LVM's with frequencies of 2121 and 2144 cm^{-1} at 10 K.[8,12,16] The defect decays at temperatures above 250 °C in proton-implanted material. There is a controversy on the EPR signal of the defect. Identification of the EPR signal from an excited state (spit triplet) of VH_2^0 by Chen *et al.*[11] was later challenged by Johannesen.[17]

VH_3: The defect is paramagnetic in the neutral charge state and has C_{3v} (trigonal) symmetry.[18] Such a high symmetry implies that two of the three possible stretch modes are degenerate. Two Si–H stretch modes at 2166 and 2191 cm^{-1} (10 K measurements) were ascribed to VH_3.[8,10,12] However, the isochronal annealing behavior of the two modes differs from that of VH_3^0, determined from EPR.[18] Therefore, these modes were tentatively reassigned to the hydrogen-saturated divacancy, V_2H_6.[16,19] Recently, it has been suggested that LVM's at 2155 and 2185 cm^{-1} originate from VH_3.[19]

VH_4: The defect has T_d (cubic) symmetry, three of the four possible stretch LVM's are degenerate, and the fourth is infrared inactive.[12] In agreement with theoretical predictions, the LVM's frequencies of VH_4 are the highest for all VH_n defects: At 10 K the threefold-degenerate T_2 stretch mode lies at 2223 cm^{-1}. The infrared-inactive A_1 mode was predicted to be at 2257 cm^{-1}, from a vibrational model based on parameters obtained from a fit to the observed LVM's of VH_4, VH_3D, VH_2D_2, VHD_3, and VD_4.[12] The defect is stable up to 500 °C.

First Raman measurements on hydrogen-related defects in silicon were made on remote plasma hydrogenated samples.[20] A few Raman bands in the region 2000–2200 cm^{-1} were found and interpreted as hydrogen-related stretching modes of an extended defect called a platelet. In this work we report on a Raman spectroscopy study of proton-implanted silicon. In our study, we are able to identify LVM's of different VH_n defects. Due to another selection rule, Raman spectroscopy gives a possibility to probe LVM's, which are not active in infrared absorption, and, thus, in combination with IR absorption and EPR studies obtain information on the properties of the hydrogen-related defects in silicon.

II. EXPERIMENT

The silicon samples used in this study were *n*-type, phosphorus-doped, Cz (100) wafers with resistivity of either 2 or 0.75 Ω cm. Different room-temperature ion implantation procedures were employed in order to create VH_n in our samples. Implantation doses varied from 1×10^{16} to 2.5×10^{16} cm^{-2}. The 0.75 Ω cm samples were implanted through 30-μm-thick aluminum foil either with 1650 keV

protons or with 2100 keV deuterons. With this configuration the stopping range for the ions was within 5 μm from the sample surface. The 2 Ω cm samples were implanted either with 129 keV H_2^+ or H_2^+ and boron B^+. The irradiation dose of B^+ was 5×10^{14} cm^{-2}. The background pressure in the vacuum chamber was better than 10^{-4} torr. Boron coimplantation had no qualitative influence on the Raman spectra and was used only to increase the amount of vacancies. In order to study the thermal stability of the Raman lines a few samples were then annealed at 400 °C in air. The annealing time varied from 2 min to 11 h.

Raman measurements were performed with the 488 nm line of an Ar-ion laser for excitation. The focused incident laser beam made an angle of 40° with the sample normal. The laser power was ~300 mW and the spot size was 50 μm on the sample surface. The backscattered light was dispersed using a 0.3-m single grating spectrometer and detected with a cooled silicon charge coupled device (CCD) detector array, the sensitivity of which over the whole spectroscopic region of interest remained constant within 5%. The positions of the lines in the spectra were calibrated by the Raman lines of atmospheric N_2 and O_2. The spectral resolution was 7 cm^{-1}. Higher-resolution measurements did not further resolve the observed Raman lines. An appropriate holographic notch filter was used to reduce the scattered laser light. Low-temperature measurements were performed down to 10 K in a cold finger cryostat. Polarized Raman spectra were collected in a pseudobackscattering geometry. The polarization geometry is defined with respect to the sample surface (100): the *x*, *y*, and *z* axes are parallel to [100], [010], and [001], while y' and z' axes are parallel to $[01\bar{1}]$, and [011]. In the notation $[a(b,c)d]$, $a(d)$ refers to the propagation vector of the incident (scattered) light, while $b(c)$ refers to the polarization vector of the incident (scattered) light. Polarized spectra were corrected for differences in grating efficiency by calibration with a white light source.

III. RESULTS

Figure 1 shows typical room-temperature Raman spectra measured on the hydrogen-implanted silicon. Label *a* refers to the as-implanted sample, while label *b* to the sample annealed at 400 °C. It follows from the figure that the implantation gives rise to a number of Raman lines in a range of 1900–2250 cm^{-1}, which is characteristic of Si–H stretch LVM's. Indeed, in the deuterium-implanted sample, all these lines shift downwards in frequency by approximately a factor of $\sqrt{2}$, which proves that these are LVM's of hydrogen-related defects. The most prominent lines in the spectrum of the as-implanted sample are those at 1923, 1980, 2022, 2060, 2120, 2180, and 2234 cm^{-1} as well as a broadband centered at ~2000 cm^{-1}. As can be seen from Fig. 1(b), annealing at 400 °C removes the lines at 1923, 1980, 2022, and 2060 cm^{-1} from the spectrum and makes those at 2180 and 2234 cm^{-1} much stronger.

Careful investigation of the spectra shows that the lines at 2234, 2180, and 2120 have weak satellites located at 2205, 2155, and 2099 cm^{-1}, respectively (see the inset in Fig. 1). The relative intensities within each pair of these lines do not depend on the sample and implantation dose, as well as annealing temperature. Based on these findings we identify each pair of the lines as LVM's originating from the same defect.

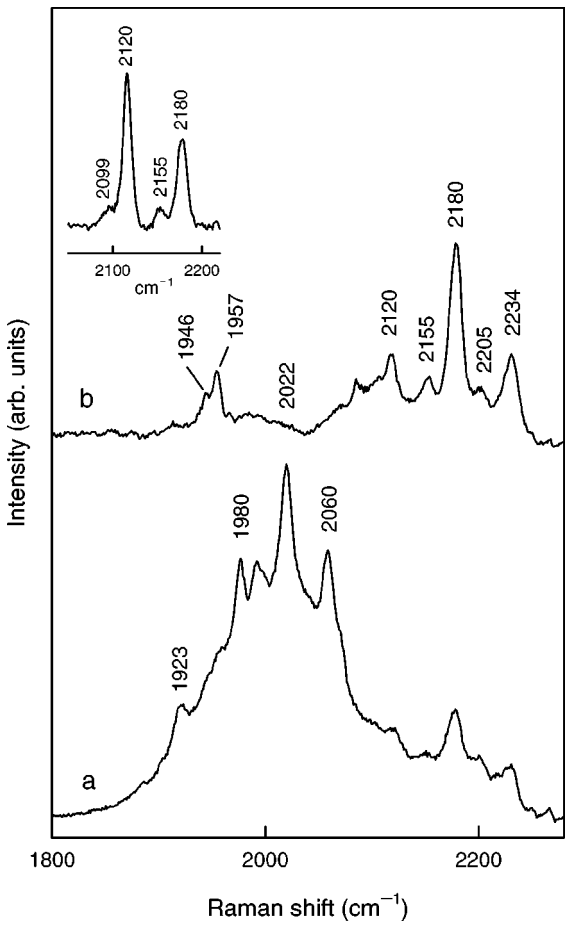

FIG. 1. Raman spectra measured at room temperature on the H_2-implanted sample: (a) as-implanted sample, (b) after annealing at 400 °C for 2 min. Spectra are offset vertically for clarity.

Polarized Raman spectra measured on the sample annealed at 400 °C and as-implanted sample are presented in Figs. 2 and 3, respectively. A more detailed analysis of these spectra will be given in Sec. IV A. Here we only note that all Raman lines have maximum intensity in the $[\bar{x}(z',z')x]$ geometry, whereas in the $[\bar{x}(z',y')x]$ geometry they are very weak or nearly absent. This result may be understood if we assume that the majority of defects responsible for these Raman lines are vacancy-hydrogen complexes. As was mentioned in the Introduction, Si–H bonds comprising these defects point almost in $\langle 111\rangle$ direction. Because LVM spectroscopy probes the local trigonal symmetry of the Si–H bonds, this implies, according to the selection rules, maximal intensity in the $[\bar{x}(z',z')x]$ and zero intensity in the $[\bar{x}(z',y')x]$ geometry.[21]

IV. DISCUSSION

A. Assignments of the Raman lines

2205- and 2234-cm^{-1} lines. The two lines have the highest frequencies of all hydrogen-related Raman modes in our

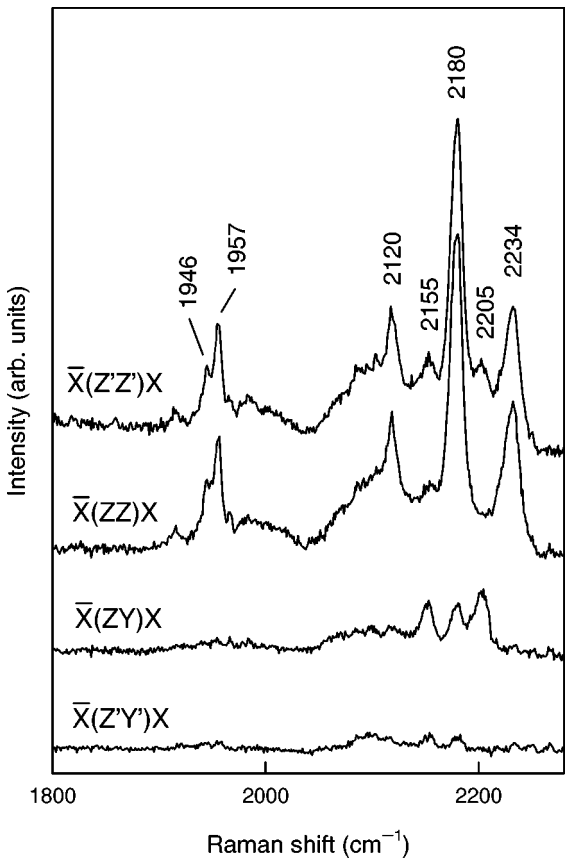

FIG. 2. Polarization Raman spectra measured at room temperature on the H_2-implanted sample after annealing at 400 °C for 2 min. Polarization geometry is defined with respect to the sample normal [001]. Spectra are offset vertically for clarity.

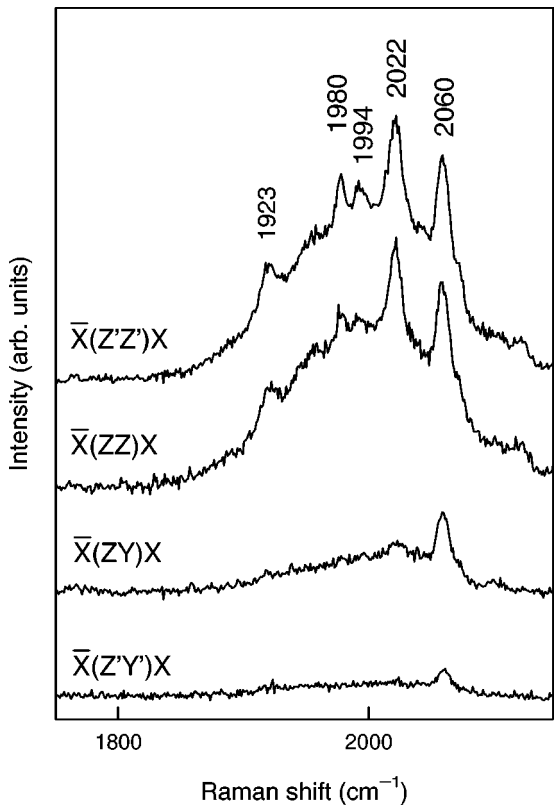

FIG. 3. Polarization Raman spectra measured at room temperature on the H_2 as-implanted sample. Polarization geometry is defined with respect to the sample normal [001]. Spectra are offset vertically for clarity.

samples. The defect responsible for them is stable up to 400 °C. At 10 K, the position of the 2205-cm^{-1} line (2223 cm^{-1}) coincides with that of the T_2 mode of VH_4, whereas the frequency of the 2257-cm^{-1} line coincides with that predicted for the infrared inactive A_1 mode of VH_4.[12] It follows from the polarized spectra (see Fig. 2) that the intensity of the 2234-cm^{-1} line is maximum in the $[\bar{x}(z',z')x]$ and $[\bar{x}(z,z)x]$ geometries and equals zero in the $[\bar{x}(z',y')x]$ and $[\bar{x}(z,y)x]$ geometries, whereas intensity of the 2205-cm^{-1} line is maximum in the $[\bar{x}(z',z')x]$ and $[\bar{x}(z,y)x]$ geometries and equals zero in the $[\bar{x}(z',y')x]$ and $[\bar{x}(z,z)x]$ geometries. According to the selection rules for polarized Raman scattering, these properties are characteristic for the A_1 and T_2 modes of a cubic defect.[21] Based on all these properties we assign the 2205- and 2234-cm^{-1} lines to the T_2 and A_1 modes of VH_4.

2155- and 2180-cm^{-1} lines. The defect responsible for the two lines is stable up to 400 °C. At 10 K the 2155- and 2180-cm^{-1} lines shift upwards in frequency to 2165 and 2190 cm^{-1}, respectively, which is very close to the infrared absorption lines previously assigned to the *E* and *A* modes of V_2H_6.[16] The polarization properties of the 2155- and 2180-cm^{-1} lines give support for the identification of the two lines as LVM's of V_2H_6 (see Fig. 2): The intensity of the 2180-cm^{-1} line is maximum in the $[\bar{x}(z',z')x]$ geometry and is reduced by more than 95% in the $[\bar{x}(z',y')x]$ geometry, whereas the 2155-cm^{-1} line is most intense in the $[\bar{x}(z',z')x]$ and $[\bar{x}(z,y)x]$ geometries and is much weaker in the $[\bar{x}(z',y')x]$ and $[\bar{x}(z,z)x]$ geometries. This is what is expected for the *A* and *E* modes of a trigonal defect. Note that slight misalignment of the sample gives nonzero intensity of the 2180-cm^{-1} line in the $[\bar{x}(z',y')x]$ geometry, which in perfect case should be zero, according to the selection rules for the *A* mode of a trigonal defect.[21]

The point group of V_2H_6 is D_{3d}, which implies that such a defect should possess four LVM's, labeled A_{1g}, E_g, A_{2u}, and E_u. The ungerade modes A_{2u} and E_u are active in infrared absorption, whereas the gerade modes A_{1g} and E_g are active in Raman scattering. The fact that the frequencies of the modes detected in Raman spectroscopy and infrared absorption are very close is consistent with our expectations. The repulsion between hydrogen atoms residing in the same vacancy is substantial and gives a dominant contribution to the ~25-cm^{-1} splitting between the gerade (and ungerade) *E* and *A* modes. However, the repulsion between two hydrogen atoms in two different vacancies will be much less due to the substantial large separation distance between the hydrogen atoms. The splitting between the gerade and the ungerade modes originates from the interaction between hydro-

gen atoms in different vacancies. Hence, a small splitting is expected in accordance with our observations.

2099- and 2120-cm^{-1} lines. The defect responsible for the two lines is stable up to 400 °C. At 10 K the 2099- and 2120-cm^{-1} lines shift upwards in frequency to 2121 and 2144 cm^{-1}, respectively, which coincide, within the accuracy of our setup, with the infrared absorption lines previously assigned to the B_1 and A_1 modes of VH_2.[8,12] Unfortunately, the rather weak intensities of the two lines in our polarized Raman spectra did not allow us to determine the symmetry of the defect. However, our data (see Fig. 2) do not contradict the C_{2v} (orthorhombic I) point group expected for VH_2. Therefore, it would be quite tempting to identify the 2099- and 2120-cm^{-1} lines as LVM's of VH_2. However, thermal stability of the defect is not in favor of this assignment: According to the FTIR absorption data,[8,12] VH_2 decays at temperatures above 250 °C, while the 2099- and 2120-cm^{-1} lines are present in the spectra after annealing at 400 °C. Nevertheless, direct comparison with the FTIR data should be made with some care, because the doses employed in FTIR absorption studies were at least one order of magnitude less compared to ours, which may give a difference in thermal stability of the defect. Another explanation of the discrepancy in thermal stability of the 2099- and 2120-cm^{-1} lines and that of VH_2 could be that the defect responsible for these lines is VH_2 perturbed by VH_n ($n=1,2,3$) rather than VH_2.[19] Thus, both FTIR absorption and Raman scattering measurements made on the same sample are needed to investigate whether the two lines originate from VH_2. Therefore, at this stage, we can only tentatively assign the 2099- and 2120-cm^{-1} lines to the LVM's of VH_2.

2022-cm^{-1} line. The defect responsible for this line decays at 400 °C. The position of the 2022-cm^{-1} line in the spectra measured at 10 K (2038 cm^{-1}) coincides with the infrared absorption line tentatively assigned to a LVM of VH^0.[15] Our polarization Raman measurements give support to this assignment (see Fig. 3): The 2022-cm^{-1} line is most intense in the $[\overline{x}(z',z')x]$ geometry and is reduced by more than 95% in the $[\overline{x}(z',y')x]$ geometry, which suggests the A mode of a trigonal defect. We note that according to the EPR data, the symmetry of VH in the neutral charge state is monoclinic I, rather than trigonal.[13,14] However, the deviation from trigonal symmetry is small and, moreover, the defect reorients swiftly well below room temperature so that the effective symmetry at room temperature is trigonal.

B. Intensities of the Raman lines

We support the above assignments of the Raman lines by calculating their relative intensities in the spectra. Here we assume that the Raman tensor of VH_n is constructed from a proper linear combination of the Raman tensors of all Si–H bonds comprising the defect.[22] Expanding the polarizability tensor of the defect, α_{ij}, over the stretch coordinates d_k of the Si–H bonds we obtain

$$\alpha_{ij}=\alpha_{ij}^0+\sum_{k=1}^{n}\frac{\partial\alpha_{ij}}{\partial d_k}d_k+\cdots, \tag{1}$$

where n is the number of hydrogen atoms in VH_n. Here α_{ij}^0 is not related to the Raman scattering and may be omitted. We also disregard terms of higher order in d_k. The relations between the stretch coordinates d_k and the normal coordinates Q_l of the lth mode are

$$d_k=\sum_{l=1}^{n}L_{kl}Q_l, \tag{2}$$

where L_{kl} is $n\times n$ matrix. L_{kl} depends on the defect and may be easily obtained using its symmetry properties (for details see Ref. 22). For example, point group of VH_4 is T_d, which means that the defect possesses two stretch LVM's, A_1 and T_2. Accordingly, the relations between d_k and Q_l are

$$Q_{A_1}=(d_1+d_2+d_3+d_4)/2, \tag{3a}$$

$$Q_{T_2^x}=(d_1-d_2+d_3-d_4)/2, \tag{3b}$$

$$Q_{T_2^y}=(d_1-d_2-d_3+d_4)/2, \tag{3c}$$

$$Q_{T_2^z}=(d_1+d_2-d_3-d_4)/2. \tag{3d}$$

When Eqs. (2) and (1) are combined, we get

$$\alpha_{ij}=\sum_{l=1}^{n}\left(\sum_{k=1}^{n}\frac{\partial\alpha_{ij}}{\partial d_k}L_{kl}\right)Q_l\equiv\sum_{l=1}^{n}\alpha_{ij}(Q_l)Q_l. \tag{4}$$

Thus, the Raman tensor of the lth mode is

$$\alpha_{ij}(Q_l)=\sum_{k=1}^{n}\frac{\partial\alpha_{ij}}{\partial d_k}L_{kl}\equiv\sum_{k=1}^{n}A_{ij}^kL_{kl}, \tag{5}$$

where A_{ij}^k is the Raman tensor of the kth Si–H bond. Equation (5) with the further assumption that all Si–H bonds point along $\langle 111\rangle$ to the center of VH_n gives a Raman tensor of the lth stretch mode. Nonzero components of A_{ij}^k in its main axes are $\alpha_{xx}=\alpha_{yy}=\delta$, $\alpha_{zz}=1$. Here δ is the bond anisotropy defined by the ratio of the dynamic molecular polarizabilities perpendicular and parallel to the bond axis. The value of δ derived from Raman scattering studies of silane and a hydrogenated Si(111) surface is equal to 0.25.[23,24] We want to compare this value with δ obtained from our analysis of the VH_n defects. Thus, with $\alpha_{ij}(Q_l)\equiv A_l$ known and disregarding the local field corrections, we obtain the intensity of the appropriate Raman line:

$$I_{Q_l}\propto\sum_{R_k\in T_d}\left|\mathbf{e}^{out}\mathbf{R}_k^TA_l\mathbf{R}_k\mathbf{e}^{in}\right|^2, \tag{6}$$

where $\mathbf{e}^{in}$ and $\mathbf{e}^{out}$ are polarization vectors of the incident and scattered light, respectively, $\mathbf{R}_k$ is the symmetry operator of the T_d point group, and $\mathbf{R}_k^T$ is transpose of $\mathbf{R}_k$.

The LVM relative intensities of VH_n calculated from Eq. (6) are gathered in Table I. For the sake of convenience the intensities are expressed by the parameters $a=(1+2\delta)/3$ and $b=(1-\delta)/3$. The bond anisotropy δ calculated from the experimental intensities of the Raman lines is shown in Table I as well. Note that VH has only one LVM and, there-

TABLE I. Relative intensities of the local modes of VH, VH_2, VH_3 (V_2H_6), and VH_4 calculated from Eq. (6). For detailed explanations see the text.

Defect	Relative intensity in Raman scattering	δ
VH_4	$I_{A_1}/I_{T_2}=a^2/b^2$	0.34
VH_3 (V_2H_6)	$I_{A_1}/I_E=(9a^2+b^2)/8b^2$	0.34
VH_2	$I_{A_1}/I_{B_1}=(3a^2+b^2)/2b^2$	0.32
VH	$I_{[\bar{x}(z,z)x]}/I_{[\bar{x}(x,y)x]}=a^2/b^2$	0.36

fore, δ may be derived only from polarized spectra. It appears from Table I that the bond anisotropy remains nearly constant within the row identified defects and the value of δ obtained for the Si–H bond in silane and on a hydrogenated Si(111) surface is 30% lower compared to our findings.

Of course, our calculations should be considered only as an estimate. The real picture must deviate from our simple model of noninteracting Si–H bonds. Keeping that in mind, we consider the value of δ calculated from Eq. (6) as a good estimate, which gives support to our assignment of the Raman lines.

V. SUMMARY

Hydrogen-implanted silicon was studied by Raman scattering spectroscopy. From polarization and intensities of Raman lines in correlation with previous IR absorption studies and isotope substitution experiments the pairs of Raman lines at 2234, 2205 and 2180, 2155 cm^{-1} were assigned to the LVM's of VH_4 and V_2H_6, respectively. A tentative assignment we give for the 2120- and 2099-cm^{-1} lines as LVM's of VH_2 and the 2022-cm^{-1} line as LVM of VH.

ACKNOWLEDGMENTS

U. Goesele (MPI Halle) and B. Köhler (TU Dresden) are acknowledged for help with organizing the experiment. E.V.L. acknowledges the Alexander–von Humboldt Foundation for financial support and the Russian Foundation for Basic Research (Grant No. 99-02-16652).

*Also at the Institute of Radioengineering and Electronics, Mokhovaya 11, 103907 Moscow, Russia.

[1] *Hydrogen in Semiconductors*, edited by J. I. Pankove and N. M. Johnson, *Semiconductors and Semimetals*, Vol. 34 (Academic Press, San Diego, 1991).

[2] S. J. Pearton, J. W. Corbett, and M. Stavola, *Hydrogen in Crystalline Semiconductors* (Springer-Verlag, Berlin, 1992).

[3] V. A. Singh, C. Weigel, J. W. Corbett, and L. M. Roth, Phys. Status Solidi B **81**, 637 (1977).

[4] P. Deák, M. Heinrich, L. C. Snyder, and J. W. Corbett, Mater. Sci. Eng., B **4**, 57 (1989).

[5] H. Xu, Phys. Rev. B **46**, 1403 (1992).

[6] C. G. Van de Walle, Phys. Rev. B **49**, 4579 (1994).

[7] M. A. Roberson and S. K. Estreicher, Phys. Rev. B **49**, 17 040 (1994).

[8] B. Bech Nielsen, L. Hoffmann, M. Budde, R. Jones, J. Goss, and S. Öberg, Mater. Sci. Forum **196-201**, 933 (1995).

[9] Y. K. Park, S. K. Estreicher, C. W. Myles, and P. A. Fedders, Phys. Rev. B **52**, 1718 (1995).

[10] B. Bech Nielsen and H. G. Grimmeiss, Phys. Rev. B **40**, 12 403 (1989).

[11] W. M. Chen, O. O. Awadelkarim, B. Monemar, J. L. Lindström, and G. S. Oehrlein, Phys. Rev. Lett. **64**, 3042 (1990).

[12] B. Bech Nielsen, L. Hoffmann, and M. Budde, Mater. Sci. Eng., B **36**, 259 (1996).

[13] B. Bech Nielsen, P. Johannesen, P. Stallinga, K. Bonde Nielsen, and J. R. Byberg, Phys. Rev. Lett. **79**, 1507 (1997).

[14] P. Johannesen, J. R. Byberg, B. Bech Nielsen, P. Stallinga, and K. Bonde Nielsen, Mater. Sci. Forum **258-263**, 515 (1997).

[15] P. Stallinga, P. Johannesen, S. Herstrøm, K. Bonde Nielsen, and B. Bech Nielsen, Phys. Rev. B **58**, 3842 (1998).

[16] M. Budde, Ph.D. thesis, University of Århus, Denmark, 1998.

[17] P. Johannesen, Ph.D. thesis, University of Århus, Denmark, 2000.

[18] J. Byberg, S. Herstrøm, and B. Bech Nielsen (unpublished).

[19] B. Bech Nielsen *et al.* (unpublished).

[20] J. N. Heyman, J. W. Ager III, E. E. Haller, N. M. Johnson, J. Walker, and C. M. Doland, Phys. Rev. B **45**, 13 363 (1992).

[21] M. Cardona, in *Light Scattering in Solids II*, edited by M. Cardona and G. Güntherodt (Springer-Verlag, Berlin, 1982), pp. 19–172.

[22] E. Bright Wilson, Jr., J. C. Decius, and Paul C. Cross, *Molecular Vibrations* (Dover, New York, 1980).

[23] R. S. Armstrong and R. J. H. Clark, J. Chem. Soc., Faraday Trans. 2 **72**, 11 (1976).

[24] M. A. Hines, T. D. Harris, A. L. Harris, and Y. J. Chabal, J. Electron Spectrosc. Relat. Phenom. **64/65**, 183 (1993).